RSC Advances

PAPER

View Article Online
View Journal | View Issue

Cite this: *RSC Adv.*, 2024, **14**, 11891

Cell-penetrating peptides noncovalently modified red phosphorescent nanoparticles for high-efficiency imaging†

Zihan Luo,[a] Zhuofan Zhou,[a] Yiwen Pan,[a] Zece Zhu,[b] Huanxiang Yuan,[c] Yutao Li,[d] Shumin Feng,*[a] Yi Hong*[a] and Li Xu*[a]

The application of long-lived phosphorescence probes in time-resolved luminescence imaging is limited by their low quantum yield in aqueous solutions. However, sensitization of thermally activated delayed fluorescence (TADF) materials can compensate for this limitation while addressing the issue of insufficient proportion of their own long lifetime. In this study, we utilized the characteristics of phosphorescence and TADF materials simultaneously by doping the receptor iridium complex PMD-Ir into the donor TADF polymer PCzDP-20 through donor–receptor doping method, and successfully prepared highly efficient red phosphorescent nanoparticles. The quantum yield of the nanoparticles obtained by this method reaches up to 30%, and the luminescence lifetime can reach several thousand nanoseconds. Additionally, due to the low concentration doping of PMD-Ir, the risk of transition metal toxicity is greatly reduced. Furthermore, we used non-covalent modification with amphiphilic cell-penetrating peptides (CPPs) to increase the cell membrane permeability of the nanoparticles. The CPPs modified nanoparticles achieve *in vivo* confocal imaging of zebrafish and intracellular time-resolved imaging by its significantly improved bioimaging capabilities. The functional nanoparticles designing method fully utilizes the characteristics of PMD-Ir, PCzDP-20, and CPPs, solving the problems of low quantum yield and poor membrane permeability of Ir-complex nanoparticles. This will greatly promote the development of time-resolved luminescence imaging.

Received 28th February 2024
Accepted 25th March 2024

DOI: 10.1039/d4ra01531b

rsc.li/rsc-advances

Introduction

Nanoparticles with long luminescence lifetimes play an important role in time-resolved luminescence imaging (TRLI) for eliminating background fluorescence from biological tissues and other complicated samples.[1] Phosphorescence and thermally activated delayed fluorescence (TADF) are typical long-lived luminescence, which have been widely used in luminescence biological imaging.[2–4] Most phosphorescent probes and nanoparticles are based on transition metal complexes,[4–8] which have a high proportion of long-lived delayed luminescence[9–13] due to the directly radiative relaxation of excited triplet states. To avoid potential toxicity of transition metal complexes, TADF molecules were developed for biological application. However, typical TADF arises from reverse intersystem crossover of excited triplet states, and the long-lived delayed fluorescence usually has a small proportion in the whole fluorescence emission, leading to weak signals in time-gated luminescence imaging with delay times up to microseconds.[1,14–22] To take the advantages of both phosphorescence and TADF, donor-receptor doped phosphorescent nanoparticles were developed through doping phosphorescent molecules into TADF donors.[23,24] Both singlet and triplet excited states of TADF donors could transfer the energy to the phosphorescence receptors, greatly increasing the proportion of long-lived luminescence.[25] Besides, doping phosphorescence molecules in a donor can reduce the concentration of triplet states, which can help to reduce triplet–triplet annihilation and increase phosphorescent quantum yield. Also, this method can significantly reduce the amount of transition metal complexes, consequently decreasing the risk of metal toxicity.

Iridium complexes, as typical phosphorescent complexes, have been predominantly developed in time-resolved imaging due to their stable photophysical properties and diversity.[12,13,26] In our previous work,[25] several iridium phosphorescent complexes were sensitized with TADF donors to develop a class of highly efficient phosphorescent nanoparticles. However, these nanoparticles exhibited limited cell membrane

[a]*Department of Pharmacy, Hubei University of Chinese Medicine, Wuhan 430065, P. R. China. E-mail: 2997@hbtcm.edu.cn*

[b]*School of Bioengineering and Health, State Key Laboratory of New Textile Materials and Advanced Processing Technologies, Wuhan Textile University, Wuhan 430200, P. R. China*

[c]*Department of Chemistry, College of Chemistry and Materials Engineering, Beijing Technology and Business University, Beijing 100048, P. R. China*

[d]*School of Laboratory Medicine, Hubei University of Chinese Medicine, Wuhan 430065, P. R. China*

† Electronic supplementary information (ESI) available. See DOI: https://doi.org/10.1039/d4ra01531b

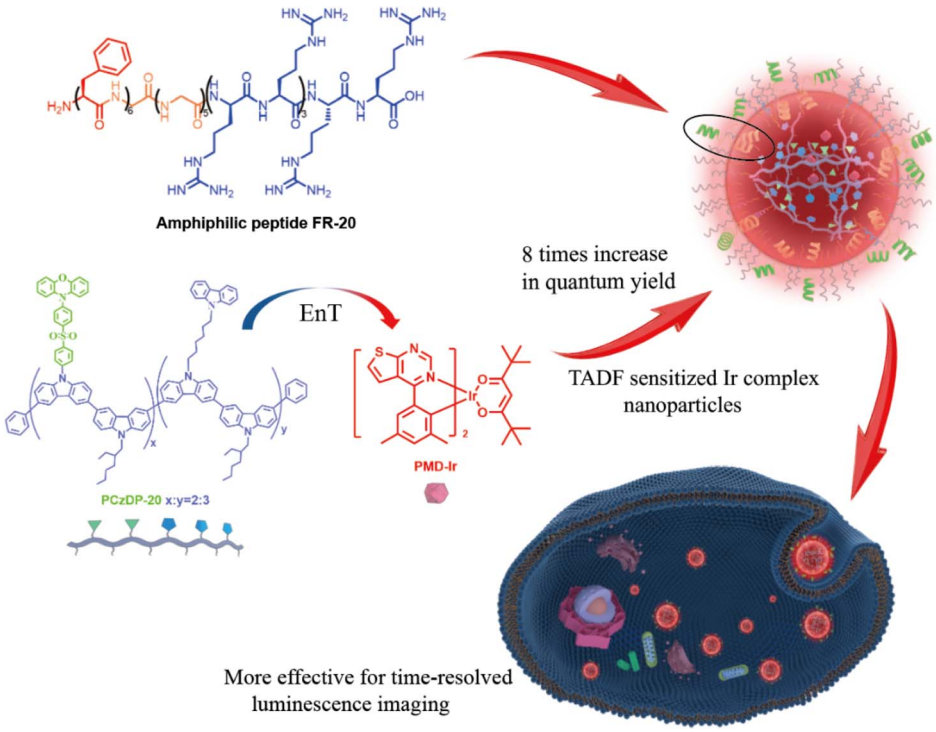

Scheme 1 Schematic representation of the formation and energy-transfer process of cell-penetrating nanoparticles assembled by PMD-Ir and PCzDP-20 with amphiphilic peptide FR-20.

permeability, resulting in long incubation times. To overcome the cell membrane barrier, cell-penetrating peptides (CPPs) were used for assembling donor-receptor doped phosphorescent nanoparticles with high luminescence intensity and long-lived lifetime in this work.[15,27–30] A thermally activated delayed fluorescence polymer (PCzDP-20) and an iridium complex (PMD-Ir) were used as the donor and the receptor respectively. In the doping system, the polymer as the donor can make the doping system more uniform, and thus make the energy transfer (EnT) more fully. Compared with the iridium complexes used in the previous work,[25] PMD-Ir exhibits longer emission wavelength and higher energy transfer efficiency take place from PCzDP-20 to PMD-Ir probably due to its lower excited triplet state level, which match better with the energy level of the PCzDP-20 donor. Due to the high energy transfer efficiency, the short-lived excited singlet states can be converted into long-lived excited triplet states, significantly enhancing the proportion of long-lifetime luminescence. Besides, the amphiphilic polypeptide FR-20 can assemble to the shell of the nanoparticles by hydrophobic interaction with the donor and receptor molecules, greatly improving the membrane permeability. These nanoparticles were successfully used for time-resolved luminescence imaging in cells and *in vivo* luminescence imaging of living zebrafish (Scheme 1).

Results and discussion

Preparation and characterization of nanoparticles

Nanoparticles in this experiment (PCzDP-20/2.5% PMD-Ir/FR-20@K.L, PCzDP-20/2.5% PMD-Ir@K.L) were simply prepared by nanoprecipitation method from PCzDP-20, PMD-Ir, amphiphilic polypeptide FR-20 and Kolliphor EL (K.L). The concentration of nanoparticles is all expressed as the concentration of PMD-Ir. The detailed preparation procedure is described in the Experimental section.

The nanoparticles were characterized by dynamic light scattering (DLS) and transmission electron microscope (TEM). As shown by the DLS results, the size of the nanoparticles ranges from 20 to 200 nm (Fig. S1†). It can be seen that the method preserves the good polydispersity of nanoparticles after CPPs modification. Meanwhile, TEM images showed the presence of aggregates of spherical particles (Fig. S2†). These results suggested that the nanoparticles can still be well encapsulated after CPPs modification.

Photophysical properties of nanoparticles

As shown in Fig. 1b, the steady-state emission of donor PCzDP-20 at 507 nm diminishes gradually with an increasing PMD-Ir doping ratio. In contrast, the steady-state emission of receptor PMD-Ir at 615 nm gradually increased. The quenching effect on PCzDP-20 was the strongest at a doping ratio of 2.5% and the energy transfer efficiency (η_{EnT}) can reach 91% at a doping ratio of 5% (Fig. 1b inset). The energy transfer efficiency is higher than that of the red emitting molecule Ir-3 (70%) in the previous work.[25] However, as shown in Fig. 1a, the steady-state luminescence spectrum of PCzDP-20 has a small spectral overlap with the absorption spectrum of PMD-Ir, so this energy transfer efficiency cannot be contributed only by the Förster mechanism. Therefore, we consider that the short-range Dexter mechanism could also be significant in the PCzDP-20/2.5%

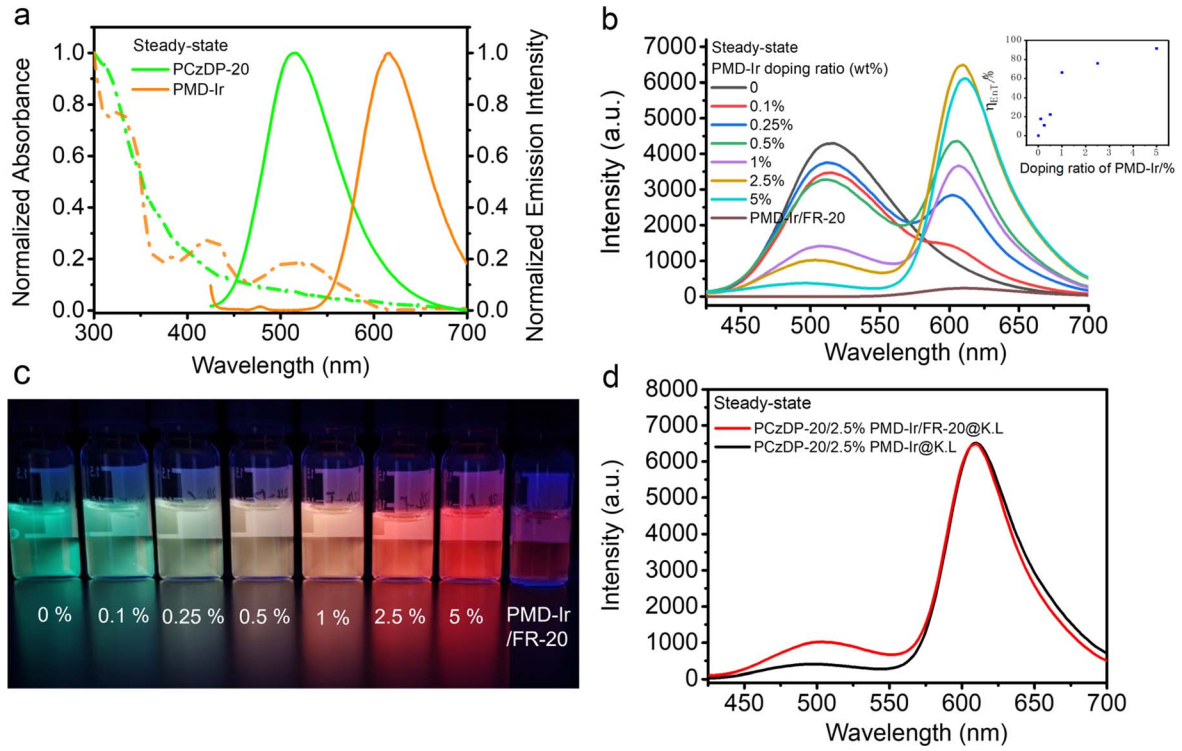

Fig. 1 (a): Absorption (dotted line) and steady-state emission spectra (solid line) of PCzDP-20 (green line) and PMD-Ir (orange line) nanoparticles in water. (b) Steady-state emission spectra of PCzDP-20/PMD-Ir/FR-20@K.L nanoparticles doped with different amounts of PMD-Ir while keeping the same amount of the TADF polymer (200 μg mL^{-1}). The inset reports the energy transfer efficiency of donor emission at 507 nm as a function of the doping ratio of PMD-Ir. (c) The image of nanoparticle solutions under UV irradiation. $\lambda_{ex} = 355$ nm; K.L: 300 μg mL^{-1}; PCzDP-20: 200 μg mL^{-1}; PMD-Ir: 0 μg mL^{-1}, 0.2 μg mL^{-1}, 0.5 μg mL^{-1}, 1 μg mL^{-1}, 2 μg mL^{-1}, 5 μg mL^{-1}, 10 μg mL^{-1}; PMD-Ir/FR-20: PMD-Ir/FR-20@K.L nanoparticles. (d) The effect of FR-20 on steady-state luminescence spectra of nanoparticles.

PMD-Ir/FR-20@K.L nanoparticles. This is consistent with the conclusions drawn from our previous work.[25]

Meanwhile, under UV excitation at 355 nm, the luminescence of nanoparticles changed from light green to red as the PMD-Ir doping ratio increases (Fig. 1c), which also demonstrated the energy transfer between PCzDP-20 and PMD-Ir. Furthermore, the steady-state luminescence intensity of the PCzDP-20 nanoparticles noncovalently modified CPPs doped with 2.5% PMD-Ir had little change at 609 nm, compared to that of unmodified CPPs nanoparticles (Fig. 1d).

The photophysical properties of PMD-Ir, PCzDP-20 and their nanoparticles, such as quantum yield, absorption wavelength and emission wavelength were summarized in Table S1.† The red-shift of the maximum emission of PMD-Ir in water compared to that in CH_2Cl_2 solution, together with a significant decrease in the quantum yield, which can be explained by its poor solubility in water. Even encapsulation of PMD-Ir by the nanoparticle shells only results in a two-fold increase in quantum yield over bare PMD-Ir in water. However, under the combined effect of PCzDP-20 and PMD-Ir, the quantum yield of nanoparticles is significantly enhanced: the quantum yield of PCzDP-20/2.5% PMD-Ir/FR-20@K.L nanoparticles is nearly 8 times higher than that of PMD-Ir/FR-20@K.L nanoparticles. Additionally, PCzDP-20/FR-20@K.L nanoparticles have the highest quantum yield, which lays the foundation for PCzDP-20 to sensitize PMD-Ir to a large extent in the energy transfer nano system. The luminescence decay was measured by time-correlated single photon counting (TCSPC). All nanoparticles exhibit multiexponential luminescence decay and show long lifetimes in the microsecond range. Time-resolved photoluminescence measurement results showed that the lifetime of PCzDP-20 decreased significantly with the increase of PMD-Ir doping ratio, as shown in Fig. 2a. With the increase of doping ratio from 0.1% to 5%, the delayed luminescence lifetime of donor PCzDP-20 decreased significantly at 520–540 nm. The triplet excited state electrons of PCzDP-20 transferred to PMD-Ir may be the reason for the shortened emission lifetime of PCzDP-20 at 520–540 nm. In addition, the PCzDP-20 nanoparticles doped with 2.5% PMD-Ir exhibit a longer luminescence lifetime compared to PMD-Ir/FR-20@K.L nanoparticles (Fig. 2b). And the average fluorescence lifetime at 615 nm increases from 102 ns to 1297 ns.[31] Both the phosphorescence lifetime and luminescence (Fig. 1b) are improved, making the nanoparticles more conducive to time-resolved luminescence imaging.

Cytotoxicity

The low cytotoxicity of nanoprobes is essential for their use in cell imaging. The imaging capability of the nanoparticles in living cells was tested using MTT (3-(4,5-dimethylthiazole-2)-2,5-diphenyltetrazole-bromide) for cytotoxicity. As shown in

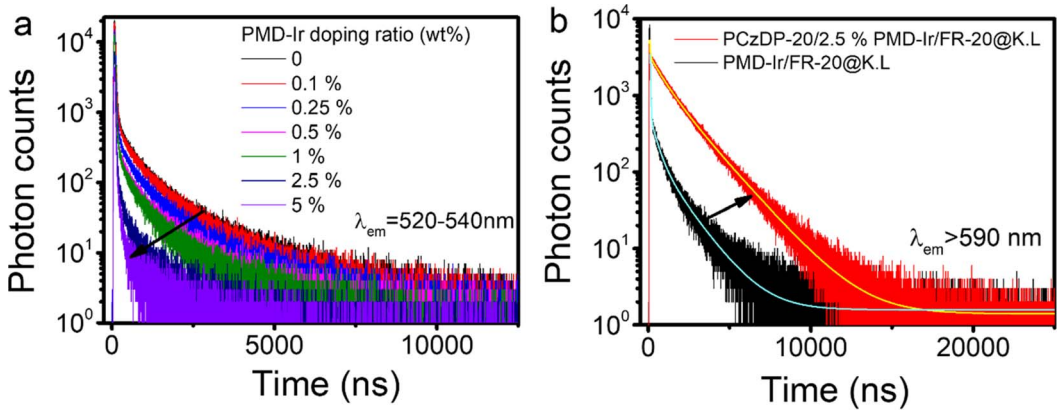

Fig. 2 (a) Lifetime decay of the PCzDP-20/PMD-Ir/FR-20@K.L nanoparticles doped with different amounts of PMD-Ir. (b) The luminescence decay curves of the PCzDP-20/2.5% PMD-Ir/FR-20@K.L and PMD-Ir/FR-20@K.L nanoparticles; [PCzDP-20] = 200 μg mL^{-1}; [PMD-Ir] = 5 μg mL^{-1}; [FR-20] = 25 μg mL^{-1}. The blue and yellow lines are fitted curves for calculating the average fluorescence lifetime. The average fluorescence lifetime is calculated from $\tau = \Sigma A_i\tau_i^2/\Sigma A_i\tau_i$.

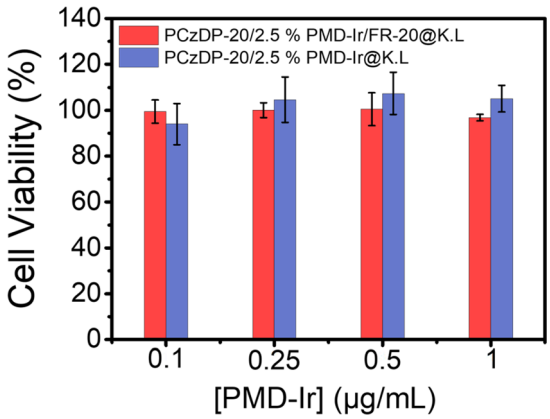

Fig. 3 Cell viability of cells after incubated at 37 °C for 24 h with PCzDP-20/2.5% PMD-Ir/FR-20@K.L and PCzDP-20/2.5% PMD-Ir@K.L.

Fig. 3, both NPs with or without amphiphilic polypeptides displayed minimal cytotoxicity, and the cell survival rate could reach over 95%. Therefore, PCzDP-20/2.5% PMD-Ir/FR-20@K.L nanoparticles can be used as biological probes for living cell imaging.

Luminescence imaging of nanoparticles in live cells

Given the excellent properties of PCzDP-20/2.5% PMD-Ir/FR-20@K.L nanoparticles, such as good water dispersion, excellent photophysical properties and low cell toxicity, we studied the application of PCzDP-20/2.5% PMD-Ir/FR-20@K.L nanoparticles in bioluminescence imaging. To highlight the role of FR-20 of nanoparticles in membrane penetration, we diluted nanoparticles by a factor of 20 (PCzDP-20: 10 μg mL^{-1}; PMD-Ir: 0.25 μg mL^{-1}) and then co-incubated with cells for 4 h at 37 °C. The result shows that the cells incubated with PCzDP-20/2.5% PMD-Ir/FR-20@K.L nanoparticles exhibited intense red emission even in ordinary fluorescence microscope (Fig. 4a), while PCzDP-20/2.5% PMD-Ir@K.L nanoparticles only showed a faint orange glow (Fig. 4c). As can be seen from Fig. 4 the luminescence of nanoparticles with FR-20 is even stronger than that of nanoparticles without FR-20. This demonstrated that FR-20 plays an important role in PCzDP-20/2.5% PMD-Ir/FR-20@K.L nanoparticles penetration into cells. It should be noted that the Ir(III) complex concentration in the nanoparticles used for cell imaging is ~0.3 μM, which is more than 10-fold lower than the incubating concentration of 5 μM for most other Ir-based bioprobes.[12,13,32–37]

In addition, from the luminescence lifetime imaging, it can be seen that the noncovalently modified CPPs nanoparticles showed luminescence lifetimes over thousands of nanoseconds in HeLa cells (Fig. 5). As a considerable portion of autofluorescence exhibits lifetimes of less than 10 ns,[38] employing time-gated detection with a delay time of 100 ns allows for efficient filtration of these fleeting fluorescence signals. The luminescence lifetimes of these nanoparticles reached over a microsecond, and the delayed luminescence can be clearly

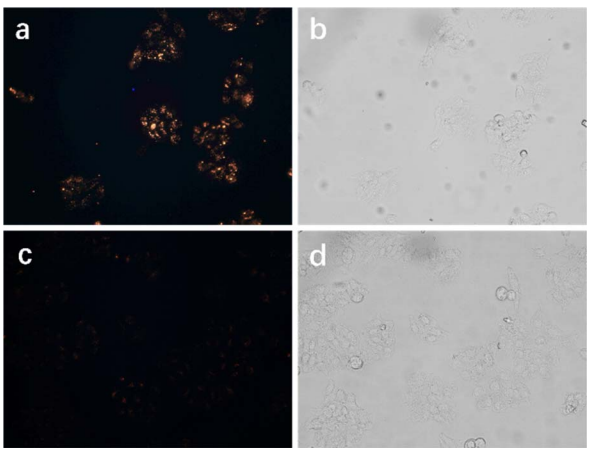

Fig. 4 Fluorescence microscope images of cells after incubation with PCzDP-20/2.5% PMD-Ir/FR-20@K.L (a and b) and PCzDP-20/2.5% PMD-Ir@K.L (c and d) for 4 h. Left, darkfield; right, brightfield.

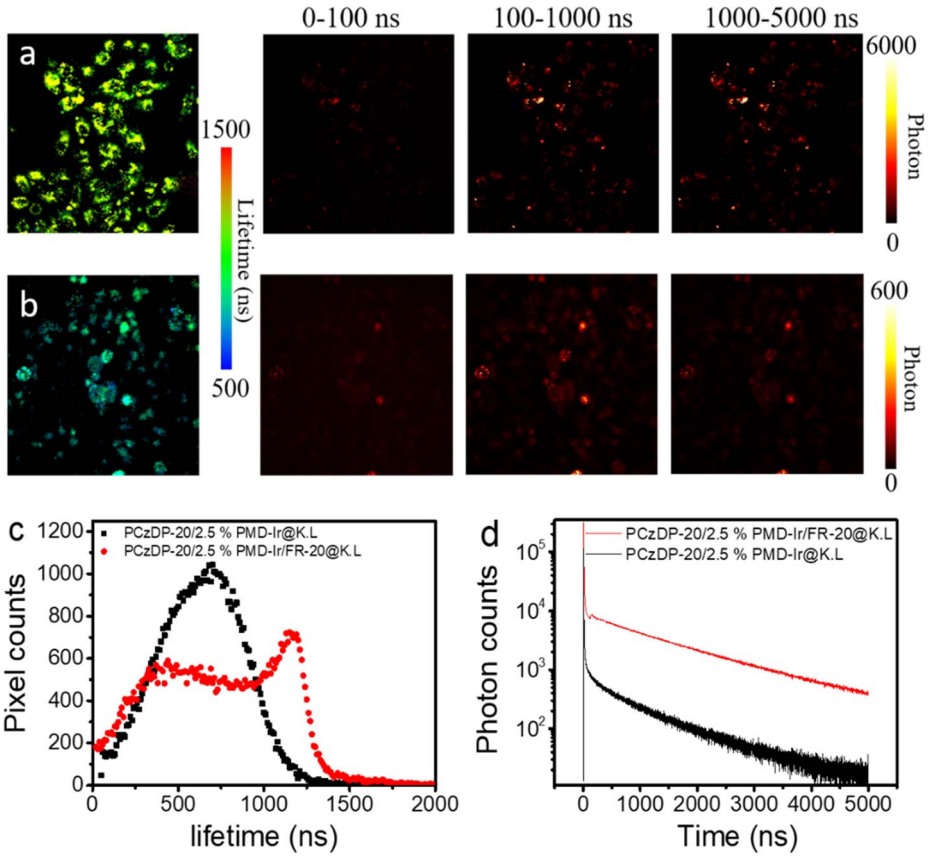

Fig. 5 Luminescence lifetime ((a) and (b)) and time-gated luminescence (red) images of (figures following (a) PCzDP-20/2.5% PMD-Ir/FR-20@K.L and (figures following (b)) PCzDP-20/2.5% PMD-Ir@K.L in HeLa cell. (c) Statistical distribution of fast lifetime from lifetime imaging and (d) the total luminescence decay curve of PCzDP-20/2.5% PMD-Ir/FR-20@K.L and PCzDP-20/2.5% PMD-Ir@K.L.

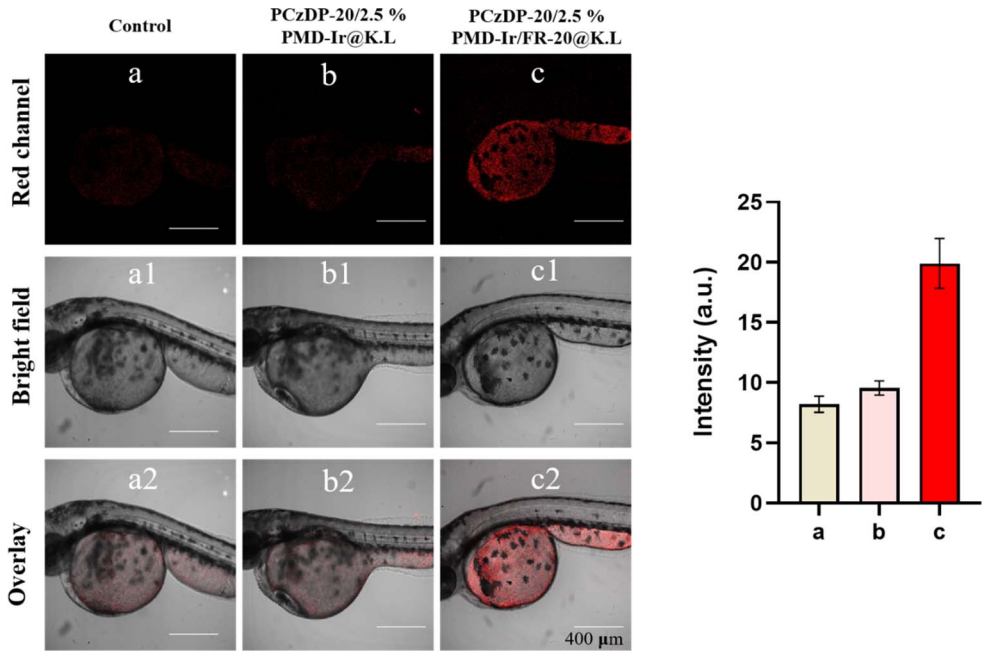

Fig. 6 Confocal images of zebrafish embryo-larvae after incubation with PCzDP-20/PMD-Ir@K.L nanoparticles for 24 h (left) and luminescence intensity collected from red channels in zebrafish larvae after incubation (right). Red channel ((a)–(c)): confocal images recorded with 580–650 nm upon excitation at 405 nm. Zebrafish embryo incubated in solution with no nanoparticles ((a)–(a2)), zebrafish embryo incubated with PCzDP-20/2.5% PMD-Ir@K.L ((b)–(b2)) and PCzDP-20/2.5% PMD-Ir/FR-20@K.L ((c)–(c2)); K.L: 15 μg mL^{-1}; PCzDP-20: 10 μg mL^{-1}; PMD-Ir: 0.25 μg mL^{-1}; FR-20: 1.25 μg mL^{-1}.

observed in the time-gated detection range of 0.1–1 μs. Even in the range of 1–5 μs, there are still obvious luminescence signals in the cells. The average lifetime statistics of luminous pixels in Fig. 5a and b is displayed in Fig. 5c. The results indicated that the majority of non-covalently modified FR-20 nanoparticles have a luminescence lifetime greater than 1 μs. Among them, the maximum value of the number of red pixel points corresponds to a luminescence lifetime of approximately 1250 ns, which is comparable to the average fluorescence lifetime of the nanoparticle solution. As shown in Fig. 5d, we constructed the luminescence decay curve of nanoparticles inside cells. We observed that at the same time point, the total photon count of nanoparticles non-covalently modified with FR-20 is ten times that of unmodified FR-20 nanoparticles. The results can be explained that compared to unmodified FR-20 nanoparticles, nanoparticles modified with FR-20 allow more nanoparticles to enter the cell, resulting in an increased number of long-lived pixels.

Luminescence imaging of zebrafish

To further demonstrate the imaging advantages of PCzDP-20/2.5% PMD-Ir/FR-20@K.L nanoparticles *in vivo*, we performed confocal imaging measurements of living zebrafish larvae. The zebrafish embryos were cared and fed in PCzDP-20/2.5% PMD-Ir@K.L nanoparticles and PCzDP-20/2.5% PMD-Ir/FR-20@K.L nanoparticles solutions respectively. Confocal imaging of zebrafish larvae after 24 h. As illustrated in Fig. 6, zebrafish larvae incubated with FR-20 unmodified nanoparticles (Fig. 6b), showed very weak luminescence, which is the same as zebrafish larvae auto luminescence (Fig. 6a). Zebrafish larvae incubated with FR-20 modified nanoparticles show that the luminescence was greatly enhanced (Fig. 6c). The luminescence intensity from zebrafish larvae incubated with FR-20 modified nanoparticles was almost doubled compared to zebrafish larvae incubated with FR-20 unmodified nanoparticles. This confirms that noncovalently modified FR-20 significantly increased the ability of nanoparticles to enter zebrafish embryos and greatly improved the visualization of luminescence imaging of zebrafish.

Conclusions

In summary, highly efficient red phosphorescent nanoparticles PCzDP-20/2.5% PMD-Ir/FR-20@K.L was designed and prepared by donor-receptor doping method and CPP modification. The nanoparticles combined the properties of PCzDP-20, PMD-Ir and FR-20, which make the nanoparticles exhibiting excellent properties for bioimaging, such as high quantum yield, long luminescence lifetime, excellent cell membrane penetration and minimal cell cytotoxicity. The nanoparticles had been used in confocal imaging of living zebrafish and time-resolved luminescence imaging in cells successfully. The functional nanoparticles developed in this work was a novel kind of optical nanomaterial, which will greatly promote the development of time-resolved luminescence imaging.

Experimental section

Materials

Kolliphor EL was purchased from Acros. FR-20 was purchased from Shanghai Dechi Biosciences Co. Ltd. HeLa cells were purchased from Procell Life Science&Technology Co., Ltd. The zebrafish embryos were purchased from Shanghai FishBio Co., Ltd. PCzDP-20 and PMD-Ir were prepared according to the previous work (see ESI† for structure, synthesis steps, and references).

Preparation and characterization of nanoparticles

PCzDP-20/2.5% PMD-Ir/FR-20@K.L nanoparticles were prepared by a simple nanoprecipitation method. Firstly, FR-20 was dissolved in Mill-Q-water with an initial concentration of 1 mg mL^{-1}, while the PCzDP-20 (8 mg mL^{-1}), Kolliphor EL (16 mg mL^{-1}) and PMD-Ir (1 mg mL^{-1}) were dissolved in THF, respectively. Then in a typical procedure, FR-20 solution (25 μL), PCzDP-20 solution (25 μL), PMD-Ir solution (5 μL) and K.L solution (18.75 μL) were mixed together and added into 1 mL distilled water. The resulting mixed solution was vigorously sonicated in ultrasonic waves (GT sonic ultrasonic cleaner) for 30 min into a final concentration of 300 μg mL^{-1} K.L, 25 μg mL^{-1} FR-20, 200 μg mL^{-1} PCzDP-20 and 5 μg mL^{-1} PMD-Ir. Finally, the aqueous solution was filtered through a 0.45 μm PVDF Syringe-driven filter. To express the energy transfer relationship between the donor and the receptor, nanoparticles were prepared with the same methods except the different amount PMD-Ir used (from 0.1% to 5% relative to 200 μg mL^{-1} PCzDP-20 donor). By the similar procedures, the nanoparticles PCzDP-20/FR-20@K.L (200 μg mL^{-1} PCzDP-20, 25 μg mL^{-1} FR-20), PCzDP-20@K.L (200 μg mL^{-1} PCzDP-20), PMD-Ir/FR-20@K.L (5 μg mL^{-1} PMD-Ir, 25 μg mL^{-1} FR-20), PMD-Ir@K.L (5 μg mL^{-1} PMD-Ir) that contain only one or two compounds were also prepared for comparison. All nanoparticle solutions were stored at 4 °C and prepared for subsequent use. Transmission Electron Microscope (TEM, HT7700, HITACHI, Inc.) and Dynamic Light Scattering (DLS, Zeta sizer Nano ZS90, Malvern, Inc.) were used to characterize nanoparticles.

Spectra measurements

UV-vis absorption spectra were recorded on a Shimadzu UV-2600 recording spectrophotometer. Steady-state for energy transfer emission spectra were measured on a Hitachi F-4600 spectrophotometer. Luminescent decay curves were measured by a single photon counting module (SPCM-AQRH-14-FC, Excelitas Technologies) equipped with a time-to-digital converter (quTAU, qutools GmbH). The samples were excited by a pulsed UV LED (370 nm; pulse width: 100 ns), and the luminescence with specific wavelength range was filtrated by optical filters.

Cell cytotoxicity

Cytotoxicity tests were performed using methyl thiazolyl tetrazolium (MTT, Sigma Aldrich) in HeLa cell lines. Briefly, logarithmic growth cells were cultured in 1×10^4 per well 96-well cell culture plates with 100 μL Dulbecco's modified Eagle's

medium (DMEM) at 37 °C and 5% CO_2 for 12 h. The cells were then incubated with PCzDP-20/2.5% PMD-Ir/FR-20@K.L nanoparticles and PCzDP-20/2.5% PMD-Ir@K.L nanoparticles for 24 hours. The MTT/PBS mixed solution was added to each well of the 96-well test plate and incubated for another 4 h. After the culture solution was removed, DMSO (200 μL) was added to each well and shook on the shaking table for 10 minutes. OD_{570} (absorbance value) was measured at 490 nm for each well using an enzyme-linked immunosorbent assay (Bio-Rad). The formula for calculating cell growth vitality is as follows:

$$\text{Viability (\%)} = (\text{mean of absorbance value of treatment group}/\text{mean of absorbance value of control}) \times 100.$$

Cell imaging

The nanoparticle dispersions were diluted with the DMEM medium to the final concentration of PMD-Ir is 0.25 μg mL^{-1}. After incubating with the diluted nanoparticle dispersions at 37 °C under 5% CO_2 for 4 h, the cells were washed with phosphate buffer saline (PBS) for several times. Luminescence imaging of live cells with the Live Cell Imaging System (PicoQuant, TRPL Mapping).

Time-resolved imaging setup is integrated with Micro Time 2000. The luminous signals were detected by the confocal microscope system equipped with TCSPC and the data were calculated using professional software provided by PicoQuant GmbH. The excitation light of 405 nm with a frequency of 0.2 MHz from the pulsed diode laser (PicoQuant, PDL 800-D) was focused onto the sample for single photon excitation.

Laser pulse excited photons were collected from a TCSPC integrated with the laser scanning confocal microscope. The sufficient number of photon events were fitted to an exponential function according to professional software provided by PicoQuant. The acquisition time of an attenuation is ~5 min. The time-gated images were obtained immediately by setting a gate time in the software to distinguish delayed and short-time luminescence as well as self-fluorescence.

Luminescence imaging of zebrafish

Zebrafish embryos were transferred into PCzDP-20/2.5% PMD-Ir/FR-20@K.L nanoparticles and PCzDP-20/2.5% PMD-Ir@K.L nanoparticles solution that diluted 20-fold with nutrient solution and incubated for 24 h at 28 °C. Then, the incubated zebrafish larvae were placed in a confocal Petri dish, washed with pure water to remove excess nanoparticles, and confocal imaging was performed. A little nutrient solution was added to the Petri dish to keep the zebrafish larvae alive.

Ethical statement

The study only involves zebrafish embryos, and there are no other experimental animals or human subjects involved in the research.

(1) All experiments were conducted in accordance with the ARRIVE guidelines.

(2) All experimental procedures were approved by the Animal Experiment Center of Hubei University of Chinese Medicine.

(3) All experiments followed institutional guidelines.

(4) The zebrafish used in the research were purchased from Shanghai FishBio Co., Ltd.

Conflicts of interest

There are no conflicts to declare.

Acknowledgements

We gratefully acknowledge financial support from the National Natural Science Foundation of China (51903081) and Wuhan Donglong Technology Co., Ltd for providing technical support in time-resolved imaging.

Notes and references

1 C. J. Christopherson, N. R. Paisley, Z. Xiao, W. R. Algar and Z. M. Hudson, Red-Emissive Cell-Penetrating Polymer Dots Exhibiting Thermally Activated Delayed Fluorescence for Cellular Imaging, *J. Am. Chem. Soc.*, 2021, **143**(33), 13342–13349.

2 D. Rota Martir and E. Zysman-Colman, Supramolecular iridium(III) assemblies, *Coord. Chem. Rev.*, 2018, **364**, 86–117.

3 L. Hua-Wei, K. Y. Zhang, W. H.-T. Law and K. K.-W. Lo, Cyclometalated Iridium(III) Bipyridine Complexes Functionalized with an N-Methylamino-oxy Group as Novel Phosphorescent Labeling Reagents for Reducing Sugars, *Organometallics*, 2010, **29**(16), 3474–3476.

4 A. Grichine, A. Haefele, S. Pascal, A. Duperray, R. Michel, C. Andraud and O. Maury, Millisecond lifetime imaging with a europium complex using a commercial confocal microscope under one or two-photon excitation, *Chem. Sci.*, 2014, **5**(9), 3475–3485.

5 L. M. Hirvonen, F. Festy and K. Suhling, Wide-field time-correlated single-photon counting (TCSPC) lifetime microscopy with microsecond time resolution, *Opt. Lett.*, 2014, **39**(19), 5602–5605.

6 B. del Rosal, D. H. Ortgies, N. Fernández, F. Sanz-Rodríguez, D. Jaque and E. M. Rodríguez, Overcoming Autofluorescence: Long-Lifetime Infrared Nanoparticles for Time-Gated In Vivo Imaging, *Adv. Mater.*, 2016, **28**(46), 10188–10193.

7 A. T. Bui, A. Grichine, A. Duperray, P. Lidon, F. Riobé, C. Andraud and O. Maury, Terbium(III) Luminescent Complexes as Millisecond-Scale Viscosity Probes for Lifetime Imaging, *J. Am. Chem. Soc.*, 2017, **139**(23), 7693–7696.

8 S. Wu, Y. Li, W. Ding, L. Xu, Y. Ma and L. Zhang, Recent Advances of Persistent Luminescence Nanoparticles in Bioapplications, *Nano-Micro Lett.*, 2020, **12**(1), 70.

9 Y. Ma, S. Liu, H. Yang, Y. Wu, C. Yang, X. Liu, Q. Zhao, H. Wu, J. Liang, F. Li and W. Huang, Water-soluble phosphorescent iridium(iii) complexes as multicolor

probes for imaging of homocysteine and cysteine in living cells, *J. Mater. Chem.*, 2011, **21**(47), 18974–18982.

10 K. Y. Zhang, H.-W. Liu, M.-C. Tang, A. W.-T. Choi, N. Zhu, X.-G. Wei, K.-C. Lau and K. K.-W. Lo, Dual-Emissive Cyclometalated Iridium(III) Polypyridine Complexes as Ratiometric Biological Probes and Organelle-Selective Bioimaging Reagents, *Inorg. Chem.*, 2015, **54**(13), 6582–6593.

11 W. Zhang, F. Zhang, Y.-L. Wang, B. Song, R. Zhang and J. Yuan, Red-Emitting Ruthenium(II) and Iridium(III) Complexes as Phosphorescent Probes for Methylglyoxal in Vitro and in Vivo, *Inorg. Chem.*, 2017, **56**(3), 1309–1318.

12 C. Zhang, M. Liu, S. Liu, H. Yang, Q. Zhao, Z. Liu and W. He, Phosphorescence Lifetime Imaging of Labile Zn2+ in Mitochondria via a Phosphorescent Iridium(III) Complex, *Inorg. Chem.*, 2018, **57**(17), 10625–10632.

13 K. Y. Zhang, T. Zhang, H. Wei, Q. Wu, S. Liu, Q. Zhao and W. Huang, Phosphorescent iridium(iii) complexes capable of imaging and distinguishing between exogenous and endogenous analytes in living cells, *Chem. Sci.*, 2018, **9**(36), 7236–7240.

14 S. Gan, J. Zhou, T. A. Smith, H. Su, W. Luo, Y. Hong, Z. Zhao and B. Z. Tang, New AIEgens with delayed fluorescence for fluorescence imaging and fluorescence lifetime imaging of living cells, *Mater. Chem. Front.*, 2017, **1**(12), 2554–2558.

15 Z. Zhu, D. Tian, P. Gao, K. Wang, Y. Li, X. Shu, J. Zhu and Q. Zhao, Cell-Penetrating Peptides Transport Noncovalently Linked Thermally Activated Delayed Fluorescence Nanoparticles for Time-Resolved Luminescence Imaging, *J. Am. Chem. Soc.*, 2018, **140**(50), 17484–17491.

16 F. Ni, Z. Zhu, X. Tong, W. Zeng, K. An, D. Wei, S. Gong, Q. Zhao, X. Zhou and C. Yang, Hydrophilic, Red-Emitting, and Thermally Activated Delayed Fluorescence Emitter for Time-Resolved Luminescence Imaging by Mitochondrion-Induced Aggregation in Living Cells, *Adv. Sci.*, 2019, **6**(5), 1801729.

17 R. Wei, L. Zhang, S. Xu, Q. Zhang, Y. Qi and H.-Y. Hu, A single component self-assembled thermally activated delayed fluorescence nanoprobe, *Chem. Commun.*, 2020, **56**(17), 2550–2553.

18 F. Fang, L. Zhu, M. Li, Y. Song, M. Sun, D. Zhao and J. Zhang, Thermally Activated Delayed Fluorescence Material: An Emerging Class of Metal-Free Luminophores for Biomedical Applications, *Adv. Sci.*, 2021, **8**(24), 2102970.

19 N. R. Paisley, S. V. Halldorson, M. V. Tran, R. Gupta, S. Kamal, W. R. Algar and Z. M. Hudson, Near-Infrared-Emitting
Boron-Difluoride-Curcuminoid-Based Polymers Exhibiting Thermally Activated Delayed Fluorescence as Biological Imaging Probes, *Angew. Chem., Int. Ed.*, 2021, **60**(34), 18630–18638.

20 Z. Zhu, Z. Luo, Y.-Q. Xie, Y. Sun, L. Xu and Q. Wu, Highly Efficient Red Thermally Activated Delayed Fluorescence Nanoparticles for Real-Time in Vivo Time-Resolved Luminescence Imaging, *Adv. Funct. Mater.*, 2024, **34**(14), 2313701.

21 X. Xiong, F. Song, J. Wang, Y. Zhang, Y. Xue, L. Sun, N. Jiang, P. Gao, L. Tian and X. Peng, Thermally activated delayed fluorescence of fluorescein derivative for time-resolved and confocal fluorescence imaging, *J. Am. Chem. Soc.*, 2014, **136**(27), 9590–9597.

22 L. Tingting, Y. Dongliang, Z. Liuqing, W. Suiliang, Z. Baomin, F. Nina, W. Lianhui, T. Youtian and H. Wei, Thermally Activated Delayed Fluorescence Organic Dots (TADF Odots) for Time-Resolved and Confocal Fluorescence Imaging in Living Cells and In Vivo, *Adv. Sci.*, 2017, **4**(4), 1600166.

23 Q. Zhang, H. Kuwabara, W. J. Potscavage Jr, S. Huang, Y. Hatae, T. Shibata and C. Adachi, Anthraquinone-Based Intramolecular Charge-Transfer Compounds: Computational Molecular Design, Thermally Activated Delayed Fluorescence, and Highly Efficient Red Electroluminescence, *J. Am. Chem. Soc.*, 2014, **136**(52), 18070–18081.

24 J. Zhang, R. Chen, Z. Zhu, C. Adachi, X. Zhang and C.-S. Lee, Highly Stable Near-Infrared Fluorescent Organic Nanoparticles with a Large Stokes Shift for Noninvasive Long-Term Cellular Imaging, *ACS Appl. Mater. Interfaces*, 2015, **7**(47), 26266–26274.

25 L. Xu, J. Wang, Q. Q. Luo, G. C. Chen, F. Ni, Z. C. Zhu, Q. Zhao, G. J. Zhang and C. L. Yang, Highly emissive phosphorescence nanoparticles sensitized by a TADF polymer for time-resolved luminescence imaging, *Mater. Chem. Front.*, 2020, **4**(8), 2389–2397.

26 L. Hao, Z.-W. Li, D.-Y. Zhang, L. He, W. Liu, J. Yang, C.-P. Tan, L.-N. Ji and Z.-W. Mao, Monitoring mitochondrial viscosity with anticancer phosphorescent Ir(iii) complexes via two-photon lifetime imaging, *Chem. Sci.*, 2019, **10**(5), 1285–1293.

27 J. Regberg, A. Srimanee and Ü. Langel, Applications of Cell-Penetrating Peptides for Tumor Targeting and Future Cancer Therapies, *Pharmaceuticals*, 2012, **5**(9), 991–1007.

28 J. D. Ramsey and N. H. Flynn, Cell-penetrating peptides transport therapeutics into cells, *Pharmacol. Ther.*, 2015, **154**, 78–86.

29 M. Mae and U. Langel, Cell-penetrating peptides as vectors for peptide, protein and oligonucleotide delivery, *Curr. Opin. Pharmacol.*, 2006, **6**(5), 509–514.

30 B. Gupta, T. Levchenko and V. Torchilin, Intracellular delivery of large molecules and small particles by cell-penetrating proteins and peptides, *Adv. Drug Delivery Rev.*, 2005, **57**(4), 637–651.

31 J. Wang, X. Gu, H. Ma, Q. Peng, X. Huang, X. Zheng, S. H. P. Sung, G. Shan, J. W. Y. Lam, Z. Shuai and B. Z. Tang, A facile strategy for realizing room temperature phosphorescence and single molecule white light emission, *Nat. Commun.*, 2018, **9**(1), 2963.

32 X. Zheng, H. Mao, D. Huo, W. Wu, B. Liu and X. Jiang, Successively activatable ultrasensitive probe for imaging tumour acidity and hypoxia, *Nat. Biomed. Eng.*, 2017, **1**(4), 0057.

33 Q. Yu, K. Y. Zhang, H. Liang, Q. Zhao, T. Yang, S. Liu, C. Zhang, Z. Shi, W. Xu and W. Huang, Dual-Emissive

Nanohybrid for Ratiometric Luminescence and Lifetime Imaging of Intracellular Hydrogen Sulfide, *ACS Appl. Mater. Interfaces*, 2015, **7**(9), 5462–5470.

34 K. Lo, K. Tsang, K. Sze, C. Chung, T. Lee, K. Zhang, W. Hui, C. Li, J. Lau and D. Ng, Non-covalent binding of luminescent transition metal polypyridine complexes to avidin, indole-binding proteins and estrogen receptors, *Coord. Chem. Rev.*, 2007, **251**(17–20), 2292–2310.

35 C. Li, M. Yu, Y. Sun, Y. Wu, C. Huang and F. Li, A Nonemissive Iridium(III) Complex That Specifically Lights-Up the Nuclei of Living Cells, *J. Am. Chem. Soc.*, 2011, **133**(29), 11231–11239.

36 L. He, Y. Li, C.-P. Tan, R.-R. Ye, M.-H. Chen, J.-J. Cao, L.-N. Ji and Z.-W. Mao, Cyclometalated iridium(iii) complexes as lysosome-targeted photodynamic anticancer and real-time tracking agents, *Chem. Sci.*, 2015, **6**(10), 5409–5418.

37 Z. Feng, P. Tao, L. Zou, P. Gao, Y. Liu, X. Liu, H. Wang, S. Liu, Q. Dong, J. Li, B. Xu, W. Huang, W.-Y. Wong and Q. Zhao, Hyperbranched Phosphorescent Conjugated Polymer Dots with Iridium(III) Complex as the Core for Hypoxia Imaging and Photodynamic Therapy, *ACS Appl. Mater. Interfaces*, 2017, **9**(34), 28319–28330.

38 K. Y. Zhang, Q. Yu, H. Wei, S. Liu, Q. Zhao and W. Huang, Long-Lived Emissive Probes for Time-Resolved Photoluminescence Bioimaging and Biosensing, *Chem. Rev.*, 2018, **118**(4), 1770–1839.